First order phase transition with the functional renormalization group method

S. Nagy[1] and J. Polonyi[2]

[1]*Department of Theoretical Physics, University of Debrecen, P.O. Box 5, H-4010 Debrecen, Hungary*
[2]*Strasbourg University, CNRS-IPHC, 23 rue du Loess, BP28 67037 Strasbourg Cedex 2, France*

(Received 17 May 2024; accepted 15 July 2024; published 9 August 2024)

The renormalization group method, more specifically the Wegner-Houghton equation, is used to find first order phase transitions in a simple scalar field theory with a polynomial potential. An improved definition of the running parameters allows us to explore the renormalization group flow down to the IR endpoint and to locate phase transitions. Beyond the expected first order transition further radiative correction generated first and second order transitions are found. The phase diagram is reviewed by a Monte-Carlo simulation of the lattice regulated version of the theory but the serious slow down of the convergence prevents us from obtaining conclusive results from the simulation.

DOI: 10.1103/PhysRevD.110.045012

I. INTRODUCTION

Phase transitions are defined as singularities in the relation between the infrared (IR) and the ultraviolet (UV) quantities of a system. The origin of the singularities is a subtle question because systems with finite number of degrees of freedom possess analytic scale dependence therefore display no phase transition. Phase transitions take place only in strictly infinite systems which are beyond our experimental and analytical possibilities hence they have to be considered as useful approximations for systems with a large but finite number of degrees of freedom.

The theoretical challenge of phase transitions is to find the origin of a singularity in the relation between the IR and the UV quantities. Field theories can be rendered finite by introducing an UV and an IR cutoff and phase transitions appear when one of these cutoffs is removed. Since the physical laws are known up to a finite spatial resolution only the IR cutoff can be removed in a realistic theory.

The best method to deal with such a problem is the renormalization group, devised just to follow the scale dependence. The renormalization group was used originally to send the UV cutoff to infinity in relativistic quantum field theory by keeping the physics fixed at a finite scale [1,2]. The method was recovered independently later in statistical mechanics to explain the emergence of power like singularities and universality at the critical points of second order phase transitions by constructing block spin variables by the decrease of the UV cutoff in finite steps, [3–5]. The relation between the two procedures was understood soon [6] and can be summarized in a simple cases of a relativistic massive quantum field theory and a spin model as follows: The models have two important scales, one is the UV cutoff, say the highest momentum Λ and the lattice spacing a in quantum field theory and lattice spin models, respectively and the other is an intrinsic IR scale, say the Compton wavelength λ_C and the correlation length ξ of the spin system. The Compton wavelength serves as a correlation length for the quantum field because a particle cannot be localized within its Compton wavelength.

The intrinsic scale separates the UV and the IR scaling regimes, defined by the cutoff dependence of physical quantities in such a manner that the cutoff-dependence is weak in the IR scaling regime. This is easiest to see in the spin system where the evolution of the parameters of the Hamiltonian during an increase of the lattice spacing is due to the fluctuations within a block with length scale between the old and the new lattice spacing. Since these parameters are usually defined as the value of some special connected Green functions, one-particle irreducible vertex functions, their evolution slows down as we enter into the IR scaling regime beyond the correlation length.

We can now return to the question of the singularities. It was found that the contributions to the relation between the UV and IR quantities pile up in an approximately scale invariant manner in the UV scaling regime. Hence the diverging length of this scaling regime, $\Lambda\lambda_C = \xi/a \to \infty$, serves as the source of the singularities of quantum field theories and critical systems.

We have surveyed the origin of the singularities in continuous phase transition to motivate the question

leading to the topic of this work: Where do the singularities of a first order phase transition with finite the correlation length come from? The pictured suggested here is that the continuous and the discontinuous phase transitions agree that the singularities emerge from the piling up fluctuations in a long scale window rather than from the dynamics at a given scale but differ in the scale window. The critical behavior comes from the UV asymptotic scaling regime. The dynamics is approximatively scale invariant here because the only scale parameter here, the cutoff, is hidden by the running of the parameters of the action. The first order phase transitions are driven by processes at a finite scale, the formation of critical droplets [7–10] but the singularities appear only after a long non scale-invariant evolution in the IR scaling regime, in the thermodynamical limit.

The goal of this work is to find a first order transition in a simple ϕ^6 Euclidean scalar model in three dimensions by the help of the renormalization group method. This method is usually employed locally, around an UV fixed point, to remove the UV cutoff from quantum field theories and establish universal critical exponents. Another fixed points such as the Wilson-Fisher [11] and the Kosterlitz-Thouless [12] have been found useful to understand the origin of separatrices in the renormalization group flow at phase boundaries. A more systematic global extension of the renormalization group flow, the global renormalization group [13], shows the richness of the scale dependence in more realistic theories with several intrinsic scales by offering different classification schemes for the same observable algebra. The proposed view of first order transitions is motivated by this approach where the emphasis lies on the scale dependence beyond a simple asymptotic scaling analysis close to a fixed point.

The renormalization group method becomes more powerful by exploiting a new small parameter, the step size of the scale change. When the gliding UV cutoff, denoted below by k, is defined in momentum space then its change Δk can be as small as $\mathcal{O}(1/L)$ in units of $c = \hbar = 1$ where L is the IR cutoff, the size of the system. The beta functions, the derivative of the running parameters with respect to k, are given by the one-loop expression in the infinitesimal blocking limit $\Delta k \to 0$ because the higher loop contributions are $\mathcal{O}(\Delta k)$ [6,14,15]. A slightly different way to use such a possibility of arriving at exact evolution equations is to give up the plan of keeping the physics independent of the running cutoff and to follow the evolution of the effective action along an artificial trajectory in the space of theories connecting a soluble theory with the physical one by the help of an IR cutoff [16].

There is an arbitrary step in setting up the renormalization group method. The point is that the running parameters of the action are not uniquely defined due to a conflict: On the one hand, the analytic form of the action must be fixed for any practical calculation, and the other hand, the elimination of degrees of freedom during the lowering of the UV cutoff induces infinitely many new terms to the action. In other words, while we can handle actions with a limited number of parameters the renormalization group keeps generating infinitely many new one. Thus the definition of the new parameters is an overdetermined problem. This is actually the strength rather than a drawback of the renormalization group method because it forces us to find an appropriate definition of few running parameters which characterize a large number of physical processes. This step, the choice of the blocking procedure in Kadanoff's scheme or the subtraction procedure in the perturbative renormalization in quantum field theory, is not unique and needs optimization.

There have already been a number of works about the use of the renormalization group method for first order phase transitions. The indication that this method can capture discontinuous phase transitions came from the finding that the radiative corrections of a gauge field generate a first order transition in superconductors [17] and in scalar quantum electrodynamics (QED) [18]. In the same time a first order transition was found in simpler models, in anisotropic cubic systems [19] and its relation to the loss of a fixed point was noted in Ref. [20]. A sufficient condition of a first order transition was identified as a fixed point with a strongly relevant operator [21]. The dynamical renormalization group was used, as well, to describe first order transitions by noncritical fixed point [22]. The essential singularities of the coexistence region can be recovered as the renormalized trajectory passes a fixed point [23]. The rounding effect of the finite size scaling on first order transition was the subject of Ref. [24]. The first order phase transition may lead to multivalued thermodynamical potential in certain approximations. In a similar manner the blocking transformation may become singular in the vicinity of first order transition [25]. This result underlines the importance of the proper choice of the subtraction procedure, our main concern here. The temperature driven first order transitions can be classified by the help of the renormalization group [26]. The functional renormalization group method was used to describe first order transitions in lattice-gas models [27] and in the Nambu-Jona-Lasinio model [28].

The evolution of the effective action during the lowering of an IR cutoff has already been used to reproduce first order phase transitions. The first order transition was located in a model with two scalar fields [29,30], in the Abelian Higgs model [31] and in a scalar matrix field model [32]. The universal susceptibilities near a weak first order transition have been considered [33], as well. The tunneling and the bubble formation mechanism underlying a first order phase transition was the focus of the works [34,35]. A part of the phase structure of the ϕ^6 scalar model discussed here has been found by the help of the traditional subtraction procedure, based at vanishing field [36].

Some higher dimensional terms in the potential have been included into the calculation in [37]. The first order transition occurring in fermionic system has been discussed [38], too.

The choice of the Wilsonian bare renormalization group scheme, used in this work, can be motivated in two different manners. While the bare Wilsonian action is evolved during the UV cutoff by keeping the physics fixed the physical content of the effective action changes due to a non-physcial ingredient of the scheme, the IR cutoff. Hence only the IR end point of the renormalized trajectory for the effective action possesses physical meaning since the IR cutoff is eliminated there. This is not a important issue close to a critical point where the universal long range dynamics is governed by the approximately scale invariant UV scaling regimes but can be a serious problem for first order transitions which are driven by large amplitude collective modes, the critical droplets, residing at a well defined scale. Another advantage of the Wilsonian scheme is the transparent way the saddle point structure emerges. The critical droplet dynamics is semiclassical and the saddle point contributions can easily be isolated in the bare renormalization group scheme. For instance the tree-level contributions to the blocking relations produces a dynamical generalization of the Maxwell-cut, a degeneracy of the potential in the mixed phase regime [39]. The effective action is convex by definition and the Maxwell-cut of the effective potential hides the semiclassical dynamics leaving no room to recover it owing to the formally exact nature of the evolution equation. The Wilsonian bare potential approaches the effective potential only as the gliding UV cutoff reaches the IR end point, $k = 0$, and the saddle point dynamics makes itself manifest when k is about the inverse critical droplet size.

We start with presentation of the appropriate choice of the subtraction point, the key to recover first order phase transitions in the IR scaling regime, in Sec. II. As a simple consistency check of the new subtraction procedure the recovery of the Wilson-Fisher fixed point is shown in Sec. III. The renormalization group flow of the new subtraction scheme generates a complicated phase structure with several radiation correction induced first and second order transitions, these results are reported in Sec. IV. Such a rich structure is unexpected and a Monte-Carlo simulation was carried out to clarify the situation. As discussed in Sec. V the simulation slows down enormously just in the interesting regions of the parameter space and it can neither prove nor disprove the predictions of the renormalization group method. Finally our results are summarized in Sec. VI.

II. SOLVING A THEORY BY THE RENORMALIZATION GROUP

The renormalization group method is used below to find the evolution of the bare action during the lowering of the UV momentum space cutoff k of an Euclidean scalar field theory given by the action

$$S[\phi] = \int d^d x \left[\frac{1}{2}(\nabla\phi(x))^2 + U(\phi(x))\right] \tag{1}$$

where the potential is a N_Uth order polynomial,

$$U(\phi) = \sum_{n=1}^{N_U} \frac{g_n}{n!}\phi^n. \tag{2}$$

The only dimension of the model is expressed in units of the initial cutoff by using the bare theory $k_i = 1$ and $g_n = g_{Bn}$ as initial condition for the lowering of k.

A. Gliding UV cutoff

The blocking in momentum space, the lowering $k \to k - \Delta k$ of the UV cutoff, is supposed to preserve the partition function

$$Z = \int D[\phi] e^{-S_k[\phi]} \tag{3}$$

hence $S_{k-\Delta k}$ is found by integrating out the modes with wave vector $k - \Delta k < |p| < k$ [14],

$$e^{-S_{k-\Delta k}[\phi]} = \int D[\phi'] e^{-S_k[\phi+\phi']} \tag{4}$$

where the field variables $\phi(x)$ and $\phi'(x)$ are nonvanishing for $|p| < k - \Delta k$ and $k - \Delta k < |p| < k$ in the momentum space, respectively. The evolution equation

$$S_k[\phi] - S_{k-\Delta k}[\phi] = -\frac{1}{2}\mathrm{Tr}\ln\left[\frac{\delta^2 S_k[\phi]}{\delta\phi'\delta\phi'}\right] + \mathcal{O}(\Delta k) \tag{5}$$

obtained by ignoring saddle points contains corrections beyond the simple one-loop expression because the loop integration is over a shell of Δk thickness in momentum space. These corrections are vanishing in the small step size limit governed by the functional differential equation

$$\partial_k S_k[\phi] = -\lim_{\Delta k\to 0}\frac{1}{2\Delta k}\mathrm{Tr}\ln\left[\frac{\delta^2 S_k[\phi]}{\delta\phi'\delta\phi'}\right]. \tag{6}$$

The right-hand side is finite since the functional trace is taken over a momentum shell of thickness Δk.

To arrive at a manageable problem one employs the only approximation of the calculation, the projection of the evolution equation onto a restricted functional ansatz space for the blocked bare action. Such a functional space is usually defined by the help of the Landau-Ginzburg double expansion in Euclidean space-time, by assuming that the field has long distance fluctuations compared to the cutoff with small amplitude. To keep our calculation as simple as possible we consider a single component scalar field theory within the local potential approximation where the bare action is assumed to be of the form (1) and (2). The value

$N_U = 6$ will be used in the numerical work with $d = 3$ and the potential is assumed to be symmetric, $g_{2n+1} = 0$, except if it is stated contrary.

B. IR effective theory

The promise of Eq. (6) is to deliver a more dilute theory with a lower cutoff which is easier to handle. To find a suitable approximation for this reduced theory we introduce an IR cutoff by placing the IR effective theory into a box of size $L = 2N_p\pi/k$, N_p being an integer cutoff parameter, equipped with periodic boundary conditions. One has N_p^d modes in the path integral (3) for the field variable

$$\phi(x) = \sum_{m_\mu=0}^{N_p-1} \phi_n e^{ip_m x} \tag{7}$$

where $p_m^\mu = 2\pi m^\mu/L$, with the action density

$$\frac{S[\phi]}{L^d} = -\frac{1}{2}\prod_{j=1}^{2}\sum_{m_{j,\mu}=0}^{N_p-1} \delta_{m_1+m_2,0} p_{m_1} p_{m_2} \phi_{m_1}\phi_{m_2} + \sum_n \frac{g_n}{n!}\prod_{j=1}^{n}\sum_{m_{j,\mu}=0}^{N_p-1} \delta_{\sum_j m_j,0}\phi_{p_{m_1}}\cdots\phi_{p_{m_n}}. \tag{8}$$

By assuming that the cutoff k is low enough and no IR singularities left we take a radical step and restricts the size to $L = 2\pi/k$ leaving a single mode ϕ_0 without kinetic energy,

$$Z = \int d\phi_0 e^{-(\frac{2\pi}{k})^d U_k(\phi_0)}. \tag{9}$$

This approximation is easier to understand in Kadanoff's real space blocking [5] where the field variable is defined on a space-time lattice and one increases the lattice spacing by a fixed ratio $a \to sa$. The blocked action, defined for the more dilute blocked lattice, is given by

$$e^{S_{as}[\phi']} = \prod_n \int d\phi_n e^{-S_a[\phi]} \prod_{n'} \delta(\phi'_{n'} - B_{n'}[\phi]) \tag{10}$$

where $B_{n'}[\phi]$ denotes the blocked field variable of the block at n'. The approximation (9) correspond to have a single site blocked lattice. One looses completely the resolution in the space-time but retains enough information in the field dynamics. This approximation motivates our next step, the choice of the blocking procedure.

C. Full potential

The traditional subtraction scheme of the local potential ansatz with an arbitrary potential $U(\phi)$ is to evaluate the evolution equation (6) at the most IR field configuration, $\phi(x) = \phi$. The result is the Wegner-Houghton equation [14],

$$\dot{U}(\phi) = -\frac{\alpha_d}{2} k^d \ln[k^2 + U^{(2)}(\phi)], \tag{11}$$

where $\alpha_d = \Omega_d/(2\pi)^d$, Ω_d stands for the d-dimensional solid angle, the dot denotes the derivative with respect to $t = \ln k/k_i$, k_i stands for the initial value of the cutoff and $U^{(n)}(\phi) = \partial_\phi^n U(\phi)$.

It is known that the bare potential at $k = 0$ agrees with the effective potential and both display the Maxwell-cut, a degeneracy in between the physical vacuums, $-|\langle\phi(x)\rangle| \le \phi \le |\langle\phi(x)\rangle|$. The Maxwell-cut characterizes the mixed phase and is driven by the tree-level zero-mode dynamics of the domain walls. Despite the possibility of having concave parts of the bare potential for $k \neq 0$ a dynamical, fluctuation driven, Maxwell-cut was found for $k \neq 0$ by a second order phase transition by solving (11) numerically [40]. The convexity of the effective potential has been demonstrated, too, by solving its evolution equation. This result has later been confirmed and a formal analogy with hydrodynamics was offered to explain the cutoff-dependence of the singularities of the potential [41–43].

One should mention a technical difficulty of finding the solution by numerical integration, namely the missing of auxiliary condition(s): The evolution equation contains second order derivatives with respect to the field requiring two auxiliary conditions for a unique solution. However there is no place for these auxiliary conditions in the renormalization group method. The problem can temporarily be circumvented by applying empty, $0 = 0$, auxiliary condition [40] or keeping the auxiliary condition of the initial condition during the evolution [41] but a satisfactory solution remains to be worked out.

The order parameter is the location of the absolute minimum of the potential ϕ_a at the IR end point, $k = 0$. Hence the solution of the Wegner-Houghton equation places the phase transition at a separatrix among the renormalized trajectories, where an infinitesimal change of the initial conditions at k_i induces finite changes at $k = 0$. Such a characterization of the phase transition is possible only in the thermodynamical limit since for a large but finite quantization box $L < \infty$ the momentum spectrum is discrete, the minimal step size at the blocking (4) is $\Delta k = \mathcal{O}(1/L)$, and there are corrections to the Wegner-Houghton equation.

D. Polynomial potential

One does not need the full form of the bare potential as long as the fluctuations are small, an assumption behind any attempt to restrict the functional evolution equation into a restricted ansatz space. We might be satisfied by the knowledge of the potential around the expectation value of the field where the potential is assumed to be analytic.

To avoid the problem posed by the dynamical Maxwell-cut one introduces a weak symmetry breaking linear term in the potential to keep the expectation value slightly in the nondegenerate region. The polynomial ansatz for the potential with a base point ϕ_b is

$$U(\phi) = \sum_{n=1}^{N_U} \frac{G_n(\phi_b)}{n!} (\phi - \phi_b)^n \tag{12}$$

and the first N_U derivatives of the Wegner-Houghton equation define the beta function of $G_n(\phi_b)$,

$$\beta_n(\phi_b) = \partial_\phi^n \dot{U}(\phi_b). \tag{13}$$

The parametrization (13) contains twice as may parameters as necessary when the potential is even, $U(\phi) = U(-\phi)$, and sometime a more economical parametrization is used which is based on the variable $\rho = \phi^2$,

$$U(\phi) = V(\rho) = \sum_{n=1}^{N_U/2} \frac{\lambda_n(\rho_b)}{n!} (\rho - \rho_b)^n, \tag{14}$$

with $\rho_b = \phi_b^2$ and $g_{2n} = \lambda_n(2n)!/n!$. But one should bear in mind that the beta functions of the two parametrizations agree only for the trivial case $\phi_b = \rho_b = 0$. The nonequivalence of the beta functions is actually expected by noting that we see different features of the right-hand side of the evolution equation

$$\begin{aligned} Z_\beta &= -\frac{\alpha_d}{2} k^d \ln[k^2 + U^{(2)}(\phi)] \\ &= -\frac{\alpha_d}{2} k^d \ln[k^2 + 2V^{(1)}(\rho) + 4\rho V^{(2)}(\rho)]. \end{aligned} \tag{15}$$

In fact, the first $N_U/2$ and the N_U derivatives of Z_β enter in the ρ and the ϕ parametrization, respectively. Another, more physical difference between the two parametrization is visible by comparing the beta functions with their perturbation expression: The usual Feynman graphs are recovered only for the ϕ parametrization since there is no Wick-theorem for the composite operator ρ.

A more constructive way to compare the two parametrizations starts by considering Z_β as the generator function of the β-functions at vanishing field,

$$\begin{aligned} Z_\beta &= \sum_{n=1}^{N_U/2} \frac{\beta_{\phi 2n}}{(2n)!} \phi^{2n}, \\ &= \sum_{n=1}^{N_U/2} \frac{\beta_{\rho n}}{n!} \rho^n, \end{aligned} \tag{16}$$

with $\beta_{\phi 2n} = \beta_{\rho n}(2n)!/n!$. The β-functions at nonvanishing field are defined by

$$\begin{aligned} \beta_{\phi m}(\phi) &= \partial_\phi^m A(\phi) = \sum_{n=[\frac{m}{2}]}^{N_U/2} \frac{\beta_{\phi 2n}}{(2n-m)!} \phi^{2n-m}, \\ \beta_{\rho m}(\rho) &= \sum_{n=m}^{N_U/2} \frac{\beta_{\rho n}}{(n-m)!} \rho^{n-m}, \end{aligned} \tag{17}$$

where $[x]$ denotes the smallest integer equal or greater than x. The use of the identity $\partial_\rho = (1/2\phi)\partial_\phi$ results

$$\beta_{\rho m}(\rho) = \sum_{n=[\frac{m}{2}]}^{N_U/2} \frac{\beta_{\phi 2n} n!}{(2n)!(n-m)!} \phi^{2(n-m)} \tag{18}$$

yielding $\beta_{\phi 2m}(\phi) \neq \beta_{\rho m}(\rho)(2m)!/m!$ for $\phi \neq 0$. The rescaling factor $(2m)!/m!$ keeps the beta functions of order $\mathcal{O}(\phi^{2m})$ equivalent however different orders are mixed when the base point is nontrivial $\phi_b \neq 0$.

Another reason we refrained from using this parametrization is our goal to incorporate a linear term in the potential, used in Sec. IV G below.

E. Optimized base points

The renormalized trajectories depend on the choice of ϕ_b owing to the nonpolynomial nature of the right-hand side of the evolution equation in $U^{(2)}$. To find the best choice of the base point one needs information about the way the parameters are used later, below the current cutoff. The simplest tree-level approximation within the blocked theory is the choice $N_p = 1$, described above in Sec. II B, where the beta functions are calculated at the absolute minimum ϕ_a of the potential. The Wegner-Houghton equation taken at the evolving minimum,

$$\dot{U}(\phi_a) = \dot{\phi}_a U^{(1)}(\phi_a) - \frac{\alpha_d}{2} k^d \ln[k^2 + U^{(2)}(\phi_a)], \tag{19}$$

yields the evolution equation

$$\dot{\phi}_a = -\frac{\beta_1}{G_2} \tag{20}$$

for the minimum and

$$\dot{G}_n = \beta_n - \beta_1 \frac{G_{n+1}}{G_2} \tag{21}$$

for the parameters of the potential. The parameters corresponding to the vanishing base point will be used frequently and are denoted by $g_n = G_n(0)$.

The guidance of the tree-level approximation in the thinned blocked theory leads to serious difficulties as soon as ϕ_a changes discontinuously during the evolution. In fact, a necessary condition of the local uniqueness of the solution of the differential equation $\dot{x} = f(x,t)$ is the continuity of the right-hand side in x. Hence the renormalized trajectory, the

integral of the evolution equation, is not unique when ϕ_a jumps. A simple numerical manifestation of this problem is the ill-defined nature of the beta functions when the absolute minimum becomes degenerate. One would have thought that this case can safely be ignored for the blocking steps $k \to k - \Delta k$ with finite Δk but such a naive argument proves to be wrong, cf. Fig. 4(b) below.

A discontinuous jump of the beta functions defined at ϕ_a is unacceptable on physical grounds, too, and more involved physical processes to be taken into account by an extension of the ansatz for the blocked action or the subtraction procedure should smear out these discontinuity. In fact, it is a basic tenet of the renormalization group method that the dynamics of any finite scale window is regular and the possible singularities of phase transitions build up from the diverging size of the scale window.

The discontinuity generated by the tree-level approximation of the thinned blocked theory can be smeared out by using the average beta functions

$$\beta_n(\phi_b) = \frac{\int D[\phi]\beta_n(\phi_b,\phi_0)e^{-S_k[\phi]}}{\int D[\phi]e^{-S_k[\phi]}}, \tag{22}$$

where ϕ_0 denotes the homogeneous component of $\phi(x)$ and $\beta_n(\phi_b,\phi_0)$ stands for the beta function obtained by expanding the Wegner-Houghton equation at ϕ_0 and transforming its beta function for the Taylor expansion parameters $G(\phi_b)$ of the potential defined to the base point ϕ_b. This average simplifies to

$$\beta_n(\phi_b) = \frac{\int d\phi_0\beta_n(\phi_b,\phi_0)e^{-(\frac{2\pi}{k})^d U_k(\phi_0)}}{\int d\phi_0 e^{-(\frac{2\pi}{k})^d U_k(\phi_0)}} \tag{23}$$

by the help of the approximation (9). A further simplification can be made by applying the saddle point approximation,

$$\beta_n(\phi_b) = \frac{\sum_j \beta_n(\phi_b,\phi_j)b_j}{\sum_j b_j} \tag{24}$$

where

$$b_j = \frac{e^{-c_s(\frac{2\pi}{k})^d U_k(\phi_j)}}{\sqrt{U_k^{(2)}(\phi_j)}}, \tag{25}$$

and the points ϕ_j are local minima of the potential, $U_k^{(1)}(\phi_j) = 0$, $U_k^{(2)}(\phi_j) > 0$. The dimensionless parameter of the subtraction procedure c_s is introduced to diagnose the sensitivity of the renormalized trajectory on the choice of the absolute minimum but its value is kept at $c_e = 1$ in the results presented below.

The transformation of the beta function to a different base point $\phi_b \to \phi_b'$ is made by the linear transformation of the Taylor coefficients,

$$G_m(\phi_b') = \sum_{n=1}^{2N_U} A_{m,n}(\phi_b' - \phi_b)G_n(\phi_b) \tag{26}$$

with

$$A_{m,n}(\phi) = \begin{cases} \frac{\phi^{n-m}}{(n-m)!} & m \le n \\ 0 & n < m \end{cases}. \tag{27}$$

This results from a direct and trivial calculation or from the introduction of the ladder matrix $S_{mn} = \delta_{n+1,m}$ with the properties $S^j_{mn} = \delta_{n+j,m}$ and $S^{N_U} = 0$ allowing us to write $A(\Phi) = e^{\Phi S}$. The average beta function at $\phi_b = 0$

$$\beta_n(0) = -\frac{\alpha_d}{2}k^d \frac{\sum_j b_j \sum_m A_{nm}(-\phi_j)\partial_\phi^m \ln[k^2 + U^{(2)}(\phi_j)]}{\sum_j b_j} \tag{28}$$

is used to integrate the evolution equation $\dot{g}_n = \beta_n(0)$.

Few remarks are in order at this point:

(1) The use of the minima assures $G_2 \ge 0$ and excludes the instability $k^2 + G_2 \le 0$ during the evolution.
(2) The summation in (28) over the different minima is needed since the approximation (9) keeps the volume finite and the vacuum unique for $k > 0$.
(3) The weighted average of the beta functions at different minima is more and more dominated by the absolute minimum as the IR end point $k = 0$ is approached. Phase transition occurs when the minima are degenerate in the limit $k \to 0$.
(4) In case of symmetric initial condition the symmetry is preserved during the evolution. Nevertheless it is advised to reinforce the symmetry with respect to $\phi \to -\phi$ and to cancel the beta functions of odd orders g_{2n+1} because the small rounding errors at small n appear as relevant and their growth in the UV scaling regime lead to the gradual loss of the symmetry.

III. FIXED POINTS

Important features of the phase structure follow from the fixed points of the evolution equation. The fixed potential satisfies the dimensionless Wegner-Houghton equation,

$$d\tilde{V} - d_\phi\tilde{\phi}\tilde{V}^{(1)} = -\frac{\alpha_d}{2}\ln(1 + \tilde{V}^{(2)}), \tag{29}$$

where $d_\phi = d/2 - 1$ denotes the mass dimension of the field and the tilde indicates that the dimension is removed by the help of the cutoff, $\phi = k^{d_\phi}\tilde{\phi}$, $g_n = k^{d-nd_\phi}\tilde{g}_n$, and $U(\phi) = k^d\tilde{V}(\tilde{\phi})$. The solutions of the fixed point equations form a two-dimensional manifold. Apart of two discrete points, the trivial Gaussian and the nontrivial Wilson-Fisher fixed points, these fixed-potentials correspond to strongly

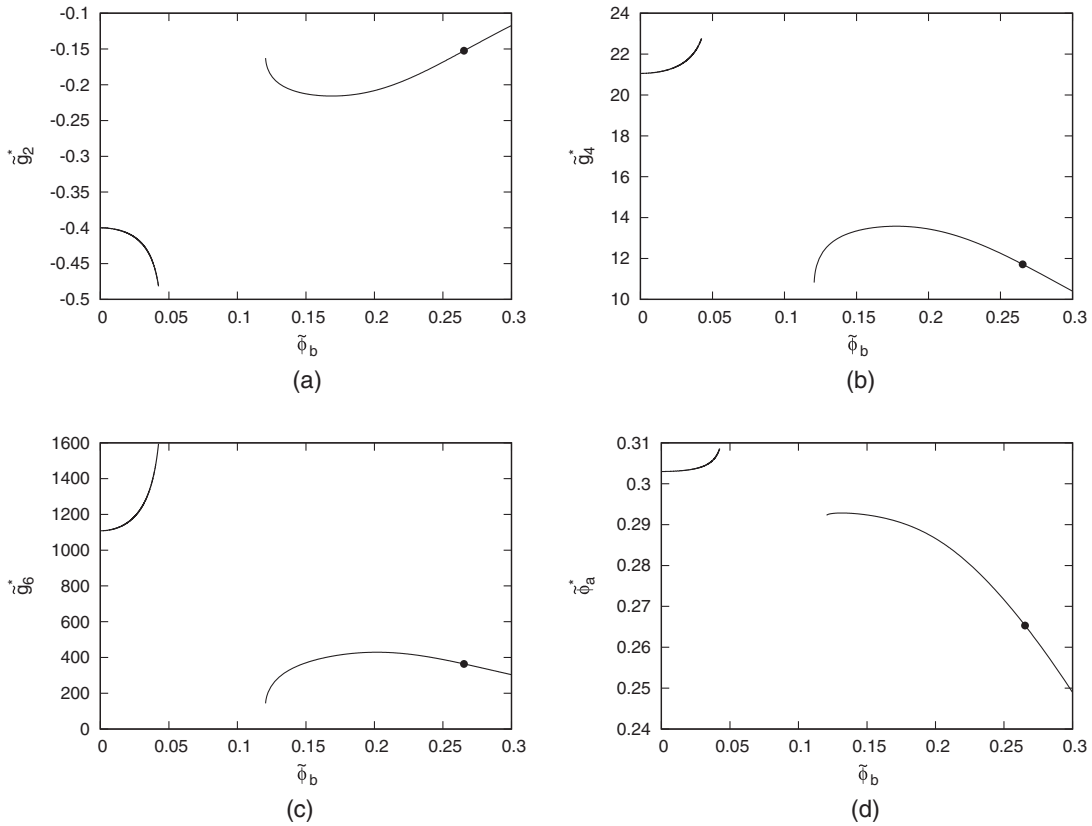

FIG. 1. The parameters of the sixth order symmetric polynomial, (a) $\tilde{g}_2^*$, (b) $\tilde{g}_4^*$, (c) $\tilde{g}_6^*$, and (d) the minimum $\tilde{\phi}_a^*$ as the function of the base point of the expansion $\tilde{\phi}_b$.

nonperturbative theories with diverging repulsion at finite particle density [44–46]. As long as our intuitive ideas about quantum field theories are taken from the perturbation expansion and its partial resummation we have to be contended by the two discrete fixed points.

The approximation of the potential by a finite order polynomial leads to the evolution equation $\dot{\tilde{G}}_n = \tilde{\beta}_n$ for the dimensionless parameters of the potential at a fixed expansion point $\tilde{\phi}_b$ and results the fixed point equation

$$(d - nd_\phi)\tilde{G}_n = \tilde{\beta}_n. \tag{30}$$

A further simplification at the fixed point where k can be arbitrarily small is that the exponential weighted beta function (28) can be replaced by the beta function calculated at the absolute minimum.

One finds easily the trivial Gaussian fixed point at $\tilde{\phi}_b = 0$. The values of $\tilde{g}_2^*$, $\tilde{g}_4^*$, and $\tilde{g}_6^*$ at the nontrivial fixed point for symmetric potential, $g_1^* = g_3^* = g_5^* = 0$, together with their minimum are shown in Fig. 1 as the function of the base point $\tilde{\phi}_b$. One finds the traditional Wilson-Fisher fixed point for $\tilde{\phi}_b = 0$. The corresponding potential has a nontrivial minimum hence this fixed point is inconsistent, its potential is obtained by expanding around an unstable base point. The extension of the fixed point, the curve leaving the Wilson-Fisher fixed point, exists for small $\tilde{\phi}_b$ and the potential becomes complex for $\tilde{\phi}_b > 0.04$, far from the actual minimum.

One can find a consistent fixed point by choosing the base point of the expansion at the minimum of the potential. The solution of Eq. (30) together with this auxiliary condition, shown by the dot in Fig. 1, can be extended for a larger interval of the base points but this manifold of solutions is substantially different than the Wilson-Fisher fixed point manifold. Hence the renormalized trajectories of the present subtraction procedure passing in the vicinity of the nontrivial fixed point are qualitatively different than the traditional one, guided by the beta functions calculated around the original Wilson-Fisher fixed point.

The fixed point Wegner-Houghton equation (29) possesses asymmetric solutions, $\tilde{V}(\tilde{\phi}) \neq \tilde{V}(-\tilde{\phi})$. However no nontrivial sixth order fixed point polynomial was found by relaxing the symmetry of the potential indicating that the critical phenomenon is strictly related to spontaneous symmetry breaking in this model.

IV. PHASE STRUCTURE

The model supports a number of phase transitions with and without spontaneous symmetry breaking with symmetric $U(\phi) = U(-\phi)$ and with full potential $U(\phi) \neq U(-\phi)$,

respectively. As of the former, there is the traditional second order phase transition with bare parameters with initial conditions $g_{B2} < 0$, $g_{B4}, g_{B6} \geq 0$. The absolute minimum of the potential depends in a continuous manner in the bare parameters around this transition hence one expects only quantitative changes compared to the traditional subtraction procedure at $\phi_b = 0$ around this transition. Therefore we devote our attention to other possible phase transitions.

A. Tree-level phase diagram

The simple rule, namely that a the term ϕ^n in the potential with larger n becomes dominant for larger values of $|\phi|$, predicts a number of tree-level phase transitions. Let us consider first a symmetric potential $U(\phi) = U(-\phi)$ where the quadratic term is dominant around zero hence the point $g_2 = 0$ is a second order transition. The higher power terms are important for larger field hence one may have first order transition if two non-Gaussian monomials compete. The stability of the model requires that the highest power come with positive coefficient hence we need at least a sixth order potential,

$$U(\phi) = \frac{g_2}{2}\phi^2 + \frac{g_4}{4!}\phi^4 + \frac{g_6}{6!}\phi^6, \tag{31}$$

with g_2, $g_6 > 0$ and $g_4 < 0$ for a first order transition. The nontrivial minima appear for $g_4 < -\sqrt{6g_2g_6/5}$ with absolute magnitude

$$\phi_m = \sqrt{10\frac{-g_4 + \sqrt{g_4^2 - \frac{6}{5}g_2g_6}}{g_6}} \tag{32}$$

which are the absolute minima as long as $g_4 < -\sqrt{8g_2g_6/5}$. The potential at the first order transition satisfies $g_4 = -\sqrt{8g_2g_6/5}$ with $G_2(\phi_m) = 4g_2$, the mass is doubled as we cross the transition line from the symmetric to the symmetry broken phase. The three dimensional parameter space (g_2, g_4, g_6) with $g_6 \geq 0$ is cut into two parts by the second and the first order transition surfaces, $g_{2\mathrm{tr}} = 0$ and $g_2 > 0$, $g_{4\mathrm{tr}} = -\sqrt{8g_2g_6/5}$, respectively. The potential is plotted on Fig. 2 for three typical set of parameters.

The appearance of a condensate in a theory with symmetric potential amounts to a spontaneous symmetry breaking. But phase transitions may occur with asymmetric potential without spontaneous symmetry breaking, too. It is easy to see for instance that one can fine tune a quartic asymmetric potential either to a critical point where the curvature at the minimum tends to zero or to a first order transition where ϕ_a jumps. The phases with and without symmetry breaking differ in the vertex structure of the fluctuations around ϕ_a. However the difference of the two phases of a theory with asymmetric potential is only quantitative since $\phi_a \neq 0$ in both cases.

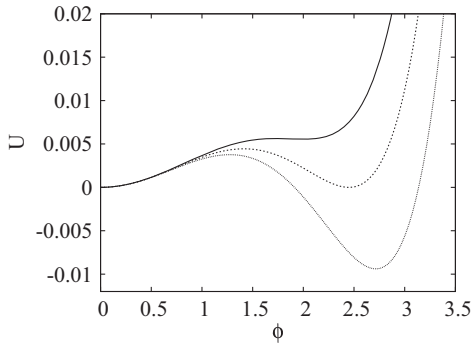

FIG. 2. The symmetric potential with $g_2 = 0.01$, $g_4 = -0.035$, -0.04, -0.045, and $g_6 = 0.1$. The minima are degenerate for $g_4 = g_{4\mathrm{tr}} = -0.04$.

The tree-level phase structure is not reliable in three dimensions since the fluctuations strongly deform the transition surface. Furthermore they generate latent heat where the order parameter is discontinuous and may produce multi-critical points. The modification of the phase structure by fluctuations is referred to as radiative corrections induced phase transitions. An additional complications of the first order transitions is that they support tree-level fluctuations, the droplet dynamics, a highly nontrivial saddle point structure. It is an interesting question whether the renormalization group evolution equation which were obtained by ignoring the possible saddle point contributions can give account of the coexistence region, dominated by the droplets.

B. Beta functions

The beta functions (13) assume a particularly simple form for a symmetric potential at $\phi_b = 0$,

$$\begin{aligned}
\beta_2(0) &= -\frac{\alpha_d}{2}k^d\frac{g_4}{k^2+g_2},\\
\beta_4(0) &= -\frac{\alpha_d}{2}k^d\frac{g_6(k^2+g_2)-3g_4^2}{(k^2+g_2)^2},\\
\beta_6(0) &= -\frac{\alpha_d}{2}k^d\frac{15g_4[2g_4^2-g_6(k^2+g_2)]}{(k^2+g_2)^3},\\
\beta_1(0) &= \beta_3(0) = \beta_5(0) = 0
\end{aligned} \tag{33}$$

allowing a qualitative understanding of the renormalized trajectories. However these beta function can not be used for strong fluctuations because the large value of the propagator around the trivial vacuum $1/(k^2+g_2)$ drives g_6 to negative values indicating a serious inconsistency of the subtraction procedure based at $\phi_b = 0$.

The instability is avoided by expanding the Wegner-Houghton equation around the minimum of the potential however this comes with a high price, the resulting beta functions are much more complicated. The expression of β_n contains the first n derivative of the right-hand side of the

Wegner-Houghton equation (11). By bringing these contributions to a common denominator one generates rather complicated expressions involving fourth order polynomials of g_2 with coefficients up to approximately 10^9. The inspection of the analytical structure confirms the triviality of the IR scaling laws below $k \approx \sqrt{G_2(\phi_a)}$ and the highly nontrivial dependence on the other parameters $G_n(\phi_a)$ suggests the existence of several further characteristic scales. The global feature of the renormalized trajectory is rendered even more complicated by the possibility that a jump of ϕ_a may place the system at the other side of such an intrinsic scale. It is not practical to reproduce the expression of the beta functions here and we content ourself with showing it for the sake of an example at the tree-level first order transition, $g_4 = g_{4\mathrm{tr}}$, calculated at the nontrivial minimum (32),

$$\begin{aligned}
\beta_1(\phi_m) &= -\alpha_d k^d 3\sqrt{3}\left(\frac{2}{5}\right)^{\frac{1}{4}} \frac{g_2^{\frac{3}{4}} g_6^{\frac{1}{4}}}{k^2 + 4g_2}, \\
\beta_2(\phi_m) &= -\alpha_d k^d \frac{1}{\sqrt{10}}(-13k^2 + 56g_2) \frac{\sqrt{g_2 g_6}}{(k^2 + 4g_2)^2}, \\
\beta_3(\phi_m) &= -\alpha_d k^d \frac{\sqrt{3}}{2^{\frac{1}{4}} 5^{\frac{3}{4}}}(5k^4 - 194k^2 g_2 + 440g_2^2) \frac{g_2^{\frac{1}{4}} g_6^{-\frac{1}{4}}}{(k^2 + 4g_2)^3}, \\
\beta_4(\phi_m) &= -\alpha_d k^d \frac{1}{10}(5k^6 - 1674k^4 g_2 + 20064k^2 g_2^2 - 32608g_2^3) \frac{g_6}{(k^2 + 4g_2)^3}, \\
\beta_5(\phi_m) &= -\alpha_d k^d \frac{\sqrt{3}}{5}\left(\frac{2}{5}\right)^{\frac{1}{4}}(-725k^6 + 32520k^4 g_2 - 210480k^2 g_2^2 + 270976g_2^3) \frac{g_2^{\frac{3}{4}} g_6^{\frac{5}{4}}}{(k^2 + 4g_2)^5}, \\
\beta_6(\phi_m) &= -\alpha_d k^d \frac{3}{\sqrt{10}}(-165k^8 - 25948k^6 g_2 - 485376k^4 g_2^2 + 2107584k^2 g_2^3 - 2256128g_2^4) \frac{\sqrt{g_2} g_6^{\frac{3}{2}}}{(k^2 + 4g_2)^3}.
\end{aligned} \tag{34}$$

The final averaged beta function

$$\beta_n(0) = \sum_m A_{nm}(-\phi_m)\beta_m(\phi_m) \tag{35}$$

can generate highly complex renormalized trajectories.

The UV and the IR scaling laws correspond to the cutoff interval where $\tilde{G}_2 = G_2/k^2 < 1$ and $\tilde{G}_2 > 1$, respectively. Hence $\tilde{G}_2$ can be considered as the measure of the IR-ness of the scaling laws. It usually increases monotonously during the evolution and the scale interval $0 < k < k_i$ is split into two parts separated by the UV-IR crossover at $\tilde{G}_2 = 1$. Another equivalent definition of the cutoff at the UV-IR crossover is $k_{\mathrm{cross}} = m$ where $m = \sqrt{G_2}$ is interpreted as the mass of the elementary excitations. The asymptotic UV and IR scaling simplifies by replacement $1/(k^2 + G_2)$ by $1/k^2$ and $1/G_2$ in the beta functions, respectively. The evolution is slow in the IR scaling regime in theories with a gap in their excitation spectrum and trivial, i.e., the only relevant operator around the Gaussian fixed point is the quadratic ϕ^2. We shall see that ϕ_a may jump during the evolution and there might be several IR scaling regimes along some renormalized trajectories.

C. Strong renormalization close to the phase boundary

The absolute minimum of the potential remains either vanishing $\phi_a = 0$ or nonvanishing $\phi_a = \phi_m$ all along the renormalized trajectories deeply within the symmetric or the symmetry broken phase, respectively. But contrary to continuous phase transitions ϕ_a may jump between 0 and ϕ_m during the evolution close to the first order phase transition. The corresponding jump of $G_2(\phi_a)$ may throw the system from one scaling regime to another rendering the global features of the renormalized trajectory, in particular the relation between the UV and the IR parameters, becomes highly involved.

This mechanism is demonstrated in Fig. 3 where the evolution of the parameters are shown close to the separatrix of the first order transition for different g_{B4} with fixed g_{B2} and g_{B6}. The tree-level transition line is at $g_{B4} = g_{4\mathrm{tr}} = -0.4$ and the trajectories with initial value $g_{B4} = -0.38, -0.39, -0.4, -0.41, -0.42$ are displayed. The evolution of g_4 is weak and smooth for $g_{B4} > -0.4$ in the symmetric phase where ϕ_a remains vanishing according to Fig. 3(a). But a violent renormalization sets in slightly below $g_{B4} = -0.4$ because the beta functions change in a discontinuous manner at $g_{B4} = -0.4$. Thus the slightest renormalization of g_2 and g_6 just below $g_{B4} = -0.4$ may induce a jump of ϕ_a along the trajectory. Actually $\beta_2(\phi_m)$ is

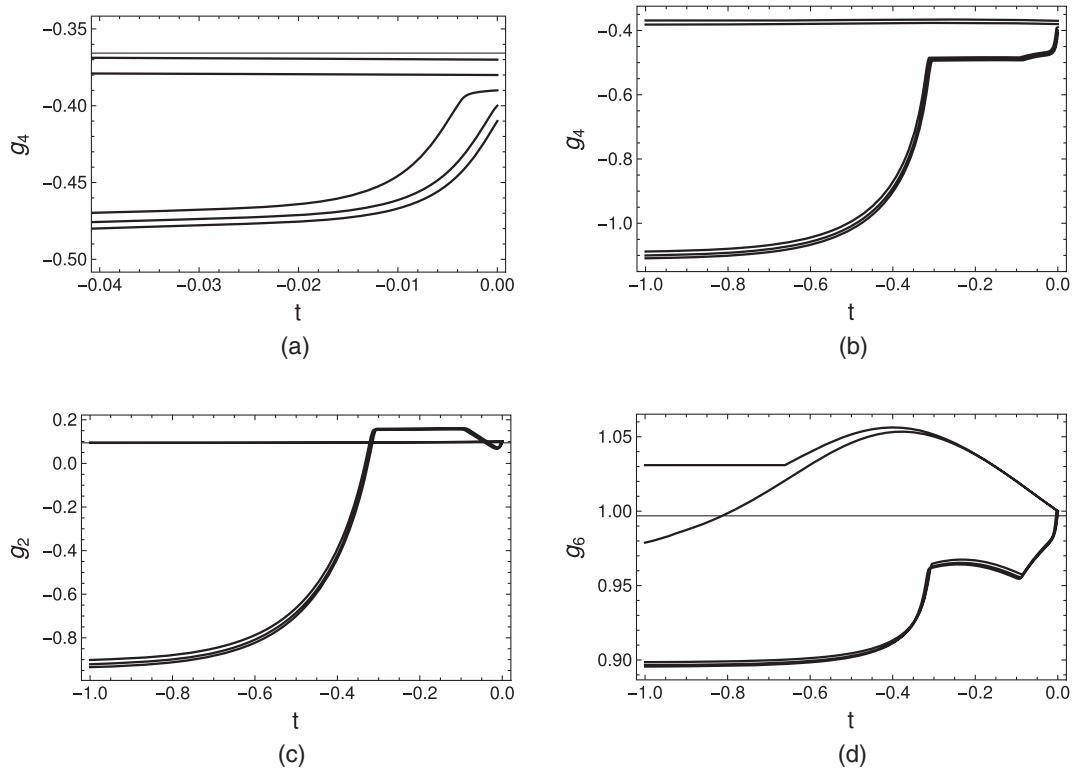

FIG. 3. The evolution of the parameters along the first order phase boundary for $g_{B2} = 0.1$, $g_{B4} = -0.38, -0.39, -0.4, -0.41, -0.42$, and $g_{B6} = 1$. (a) g_4 close to the initial cutoff, (b) g_4, (c) g_2, and (d) g_6 following a longer evolution.

slightly positive and $\beta_6(\phi_m)$ is very close to zero at $k \sim k_i = 1$ hence the tree level transition point $g_{4\mathrm{tr}}$ is increased by radiative corrections and the trajectory with $g_{B4} = -0.4$ is actually driven by $\beta_2(\phi_m)$ startig with the first infinitesimal $k \to k - \Delta k$ step. As a result the separatrix is pushed toward slightly larger g_4 values compared to the tree-level solution.

The beta functions at $\phi_a = \phi_m$ tend to be larger in absolute magnitude than the those at $\phi_a = 0$ and when ϕ_a jumps and the evolution slows down (speeds up) at the jump $\phi_a = \phi_m \to 0$ ($\phi_a = 0 \to \phi_m$). The renormalization becomes more violent immediately after a jump $\phi_a = 0 \to \phi_m$ owing to the larger beta functions. However the jump throws the system into an IR scaling regime where the renormalization slows down. Such a phenomenon is well recognizable on the trajectoires of Fig. 3 belonging to the symmetry broken phase where ϕ_a jumps twice along the trajectories and $\phi_a = 0$ for $-0.33 < t < -0.08$.

The evolution of ϕ_a and the value of the potential $U(\phi_a)$ are shown in Figs. 4(a) and 4(b) for few typical trajectories for the same initial value of g_{B2} and g_{B6} and different choice of g_{B4}. Deeply within the symmetrical ($g_{B2} = -0.2$) and the symmetry broken phase ($g_{B2} = -0.8, -1.1$) ϕ_a starts and stays at $\phi_a = 0$ and $\phi_a \neq 0$, respectively, as expected. These trajectories constitute the picture of the first order phase transition, found in earlier works [33,36], where the competition of the minima was not followed. However the minimum $\phi_a = \phi_m$ falls back to $\phi_a = 0$ in our treatment within a finite scale interval $t_1 < t < t_2$ during the evolution within the symmetry broken phase closer to the transition, at $g_{B4} = -0.5$ and -0.7.

It is important to keep in mind that the trajectories remain an analytic function of the initial conditions and of the scale k for $0 < k < k_i < \infty$ owing to the continuity of the weighted average (28) with $c_s < \infty$. The discontinuity of ϕ_a in Fig. 4(a) is a mathematical artefact without relevance for physics.

D. Locking into a degenerate potential

What is rather remarkable on Fig. 4(b) that the potential remains degenerate in a finite scale interval $0 < t_2 - t_1 < \infty$. Closer inspection of these trajectories reveals an oscillatory behavior: When $\phi_a = 0$ then the simple the beta functions evolve the potential in such a manner that $U(\phi_m) > 0$ decreases and until it becomes negative. From that on the complicated beta functions are used at ϕ_m and they push $U(\phi_m)$ back to positive values and the cycle starts again. Such an oscillation can be understood by the linearization of the beta functions around the degenerate values g_{nd},

$$\Delta\dot{g}_n = \Theta_{c_s}(\Delta g_n)\Delta\beta_n^{(+)} + \Theta_{c_s}(-\Delta g_n)\Delta\beta_n^{(-)} \qquad (36)$$

where $\Delta g_n = g_n - g_{nd}$ is the deviation from the degeneracy $g_4 = g_{4\mathrm{tr}}$, $\Theta_{c_s}(x)$ is the Heaviside function smeared in an

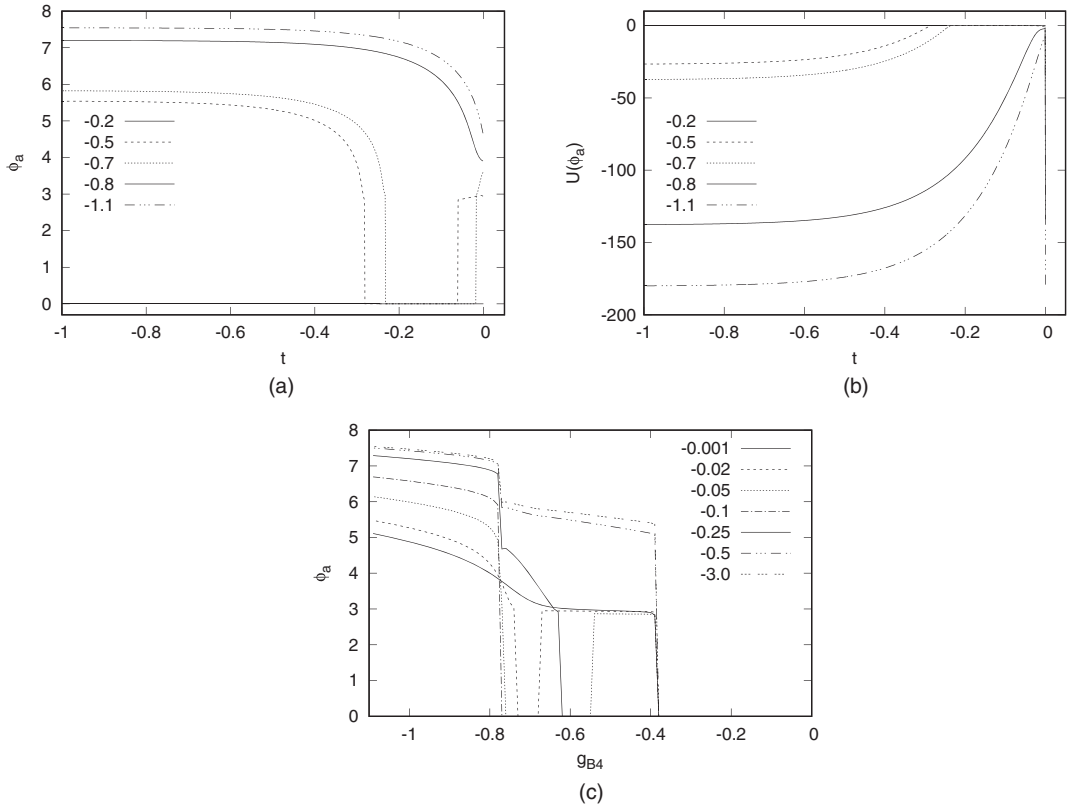

FIG. 4. The location of the absolute minimum and the value of the potential for $g_{B2} = 0.1$, $g_{B6} = 1$. (a) ϕ_a, (b) $U(\phi_a)$ as functions of the gliding scale parameter t. The values of g_{B4} are in the inset. (c) ϕ_a as the function of g_{B4}, read off at different scale parameter t, shown in the figure.

$\mathcal{O}(c_s^{-1})$ interval around zero and $\Delta\beta_n^{(\pm)}$ are continuous functions of the parameters. Such an $\mathcal{O}(\Delta k)$ oscillation of the renormalized trajectory appears to be stable against the change of the parameter c_s and is supported only in a limited scale interval $t_1 < t < t_2$ where $\pm\Delta\beta_n^{(\pm)} > 0$. The oscillation starts when the inequality sets in and stops when the ongoing renormalization leads to its violation.

Such a locking into a degenerate potential is important because the size $t_2 - t_1$ of the scale window was found to be a discontinuous function of the initial condition, g_{Bn}. Therefore the locking in mechanism generates a discontinuity between the UV and the IR parameters, namely a first order phase transition. This is shown in Fig. 4(c) where ϕ_a is plotted against g_{B4} at different scale k. The evolution is weak in the IR regime and ϕ_a at $t = -3$ can already qualitatively be treated as the order parameter which is the location of the absolute minimum at $k = 0$. The curves display two jumps in the IR scaling regime for $t < -0.5$, one around $g_{B4} = -0.38$ and another around $g_{B4} = -0.76$. The jump around $g_{B4} = -0.38$ is due to the separatrix seen in Fig. 3. The emergence of the second first order transition is due to the abrupt disappearance of the locking mechanism.

The locking of the renormalized trajectory into a degenerate potential is reminiscent of the phase mixing at the transition point. In fact, one expects that a droplet changes the dynamics when the cutoff is between size of the domain wall and the full domain. However we tend to disregard the identification of the phase coexisting region and the interval between the two fist order transitions because the former joins the two phases without first order transitions at the edges.

The strong evolution within the symmetry broken phase but close to the phase boundary generates a complicated scale dependence for ϕ_a for $t \sim 0$ around $g_{B4} = g_{\mathrm{tr}4} = -0.4$. In fact, $\phi_a = \phi_m$ during a very short evolution the but it jumps to zero on some trajectories before $t = -0.02$. The length of the scale window with $\phi_0 = 0$ is increasing during the evolution but disappears before we reach $t = -0.25$. The two jumps stabilize its position in the final IR scaling regime $t < -0.5$.

It is worthwhile noting that the weak dependence of the location of the jumps of ϕ_a on the scale k, seen in Fig. 3(c), is not an indication of weak dressing, a slow evolution along the renormalized trajectories as in the case of continuous phase transitions. What happens here is that the discrete jump of ϕ_a taking place at a certain value of k leaves a nonrecoverable impact on the trajectories and remains to be felt down to $k = 0$.

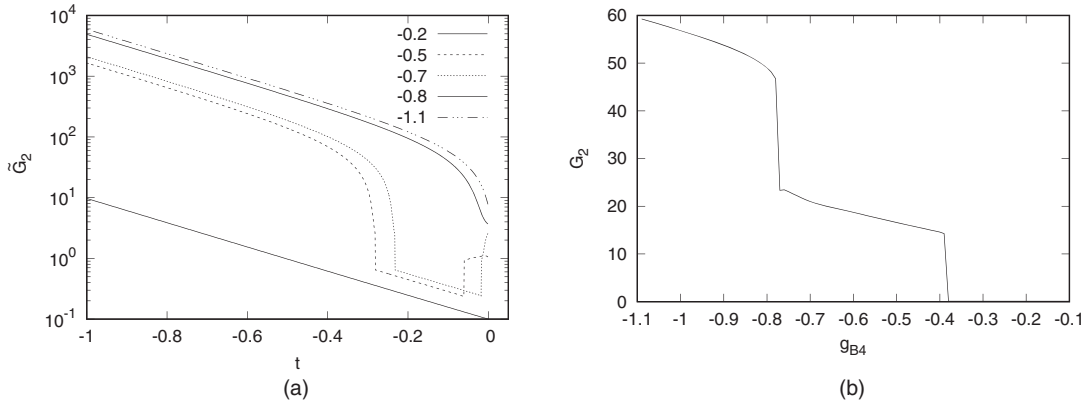

FIG. 5. (a) The evolution of $\tilde{G}_2$ and (b) G_2 deep in the IR at $t = -3$ as the functions of g_{B4} for the same value of g_{B2} and g_{B6} as in Fig. 4.

E. Quasiparticle mass

The running parameter G_2 can be interpreted with a slight abuse of the language as the mass square of the quasiparticles at the actual scale k. How does the running quasiparticle mass evolve compared to the initial cutoff k_i? We see the tree-level value of ϕ_a at the initial conditions and the mass changes by a factor two as we pass the case of degenerate initial potential. Since the location of this discontinuity is shifted very weakly there seems to be no problem to place the phase transition separating the symmetric and the symmetry broken phases at any mass at the initial condition in the symmetry broken phase.

However this picture is changed considerably according to Fig. 5. The mass square G_2 remains remarkably close to it tree-level value, $g_{B2} = 0.1$ with weak evolution along the trajectory $g_{B4} = -0.2$ in the symmetric phase where the UV-IR crossover is around $t = -0.4$ according to Fig. 5(a). But the trajectories in the symmetry broken phase suffer strong renormalization. In fact, the trajectories undergo a strong renormalization at the very beginning of the evolution close to $g_{4B} = g_{4\mathrm{tr}} = -0.4$ decreasing quickly the running mass. The mass stays approximately constant within the locking in scale window but is pushed up again by the returning of the $\phi_a = \phi_m$ scaling laws, governing the evolution from the rest of the trajectory. The IR values of G_2 is reproduced in Fig. 5(b) shows clearly that the symmetry broken theory is fully in the IR scaling regime without UV scaling laws apart of the finite locking in scale interval which exists close to the phase boundary.

Hence the free choice of the initial mass is strongly overwritten by the strong renormalization at $\phi = \phi_m$. Actually no light mass symmetry broken phase, $G_2/k_i^2 \ll 1$, was found numerically.

F. Second order transition

We have so far sought first order transitions driven by sufficiently negative g_{B4} with $g_{B2}, g_{B6} > 0$. But there might be second order transitions for less negative g_{B4}, as well. The second order spontaneous symmetry breaking of the Ising model universality class in the traditional ϕ^4 model is the result of large fluctuations around the trivial vacuum, $\phi = 0$, supported by a double well bare potential. The potential of the ϕ^6 model has local minima at ϕ_m in the symmetric phase for $-\sqrt{8g_2g_6/5} < g_4 < -\sqrt{6g_2g_6/5}$ around which finite lifetime quasiparticles can be formed. For low enough tunneling probability to the trivial minimum the life-time might be long enough to induce a second order phase transition.

A second order phase transition is indeed found in the ϕ^6 model as indicated by Fig. 6 where ϕ_a is plotted as the function of g_{B4} for $g_{2B}, g_{B6} > 0$. We are in the symmetric phase at $g_{B4} = 0$ and the moving of g_{B4} in the negative direction makes $U(\phi_m)$ smaller, the excitations around it more stable which facilitates a second order spontaneous symmetry breaking. The location of the nontrivial minimum, ϕ_m, is increased during the decrease of g_{B4} and the increasing tunneling factor brings ultimately the system back to the vicinity of the energetically favorable $\phi = 0$ by restoring the symmetry. The result is a narrows strip of symmetry broken phase within the symmetric region.

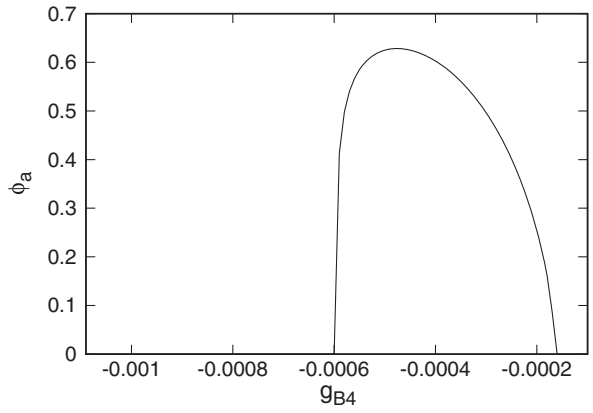

FIG. 6. The location of the absolute minimum, ϕ_a, deep in the IR at $t = -3$ as the functions of g_{B4}. The other bare parameters are $g_{B2} = 10^{-6}$ and $g_{B6} = 10^{-2}$.

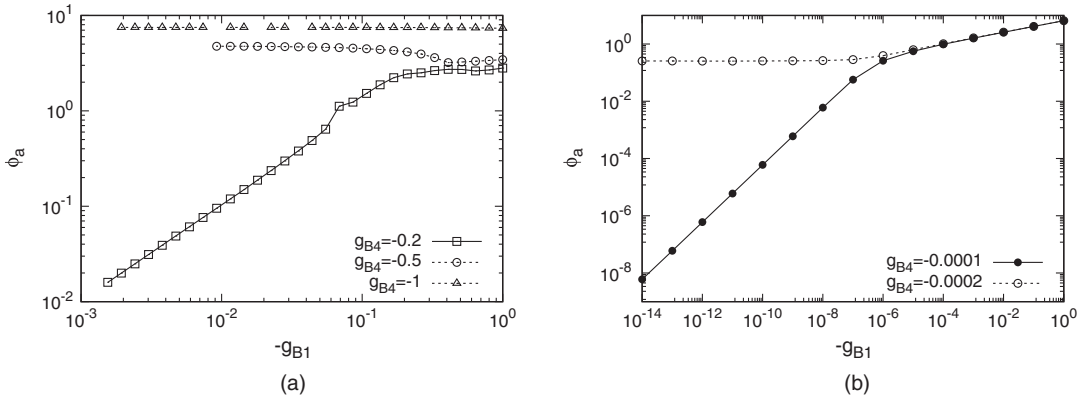

FIG. 7. The restoration of the symmetry as $g_{B1} \to 0$. (a) The first order phase transition of Fig. 4. (b) The second order phase transition of Fig. 6.

But such an explanation is very naive and can not be taken more than an educated guess. In fact, $g_{4\mathrm{tr}} = 10^{-4}\sqrt{8/5}$ for the parameters of the figure hence fluctuations must be very strong to push the first order phase transition away from $g_{4\mathrm{tr}}$ and invalidate the tree-level estimate. The first order transition was found at more negative g_{B4} but a much more detailed analysis is needed to find out whether the first and second order transitions for $g_{B2}, g_{B6} > 0$, $g_{B4} < 0$ and $g_{B4}, g_{B6} > 0$, $g_{B2} < 0$, respectively match and together separate the symmetric and the symmetry broken phases or there is a region connecting the two phases without phase transition.

G. Alternative signature of spontaneous symmetry breaking

The usual test of the ferromagnetic phase is to apply an external magnetic field and to follow the magnetization as the external field is decreased. The nonvanishing limit of the magnetization when the external field is removed is the signature of the ferromagnetic phase. Naturally the first order phase transition seen by scanning in the external magnetic field is not identical, only a related, to the second order phase transition in the temperature.

Thereby we can corroborated the phase structure by introducing a linear term in the potential, $U(\phi) \to U(\phi) + g_1\phi$, and by scanning the dependence of ϕ_a on g_{B1}. One expects a continuous g_{B1}-dependence within the symmetric phase and a discontinuity at $g_{B1} = 0$ in the phase with spontaneous symmetry breaking. The absolute minimum ϕ_m as the function of g_1, shown on the two sides of the first and the second order transition line in Fig. 7 affirms this behavior. Note that the latent heat is vanishing in these first order phase transitions.

V. LATTICE REGULARIZATION

The impressive richness of the phase structure, produced by radiative corrections, raises the question of reliability and calls for an independent check. In fact, the radiative corrections may substantially be modified by our approximation, the restriction of the blocked action space, and the choice of the subtraction procedure. A natural way to check the phase structure is to calculate the order parameter by a Monte-Carlo simulation of a lattice regulated version of the theory.

The bare action is given by the space-time sum

$$S[\phi] = \sum_n \left[\frac{1}{2}\sum_{j=1}^{3}(\phi_{n+\hat{j}} - \phi_n)^2 + g_{L1}\phi_n + \frac{g_{L2}}{2}\phi_n^2 + \frac{g_{L4}}{4!}\phi_n^4 + \frac{g_{L6}}{6!}\phi_n^6\right] \tag{37}$$

for lattice spacing $a = 1$ where vector $n = (n_1, n_2, n_3)$ with $n_j = 1, \ldots, N_L$ labels the lattice sites of an N_L^3 lattice equipped with periodic boundary conditions, $\hat{j}$ denotes the unit vector in the direction j and the partition function is given by the integral

$$Z = \prod_n \int d\phi_n e^{-S}. \tag{38}$$

A sweep of the Monte-Carlo update consists of bringing the local field into contact with a heat bath over the whole lattice in a sequential manner. The heat bath was a particular realization of the Metropolis algorithm where a shift, $\phi_n \to \phi_n + \Delta\phi$ distributed homogeneously in the interval $-\chi < \Delta\phi < \chi$, was offered to the field variable. This change was accepted with the probability $\min(1, r)$ where r denotes the ratio of the integrand of the partition function with the shifted and the original field value. This process was repeated $n_M = 6$ times before moving to the next lattice site and the parameter χ was chosen in such a manner that the acceptance ratio averaged over a sweep stayed within the interval [0.45, 0.55].

The path integral (38) has two regulators, the UV and the IR cutoffs, the lattice spacing a and the lattice size N_L,

respectively and they leave important differences compared to the partition function (3) in the continuous space-time. We intend to compare observables obtained by different regularizations thus one should determine first the bare parameters of the theory by matching some observables obtained in both calculations. This is beyond the scope of this work where we content ourself to compare the qualitative features of the phase structure.

To minimize the lattice artefacts the correlation length in lattice spacing units ξ/a should be large. The correlation lengths, the Compton wavelength of the lightest particle created by the local field, is found by projecting the field variable onto the vanishing spatial momentum sector, $\varphi_{n_1} = \sum_{n_2,n_3} \phi_n$ and calculating the connected correlation function

$$G^{(0)}_{n_1-n_1'} = \langle \varphi_{n_1} \varphi_{n_1'} \rangle - \langle \varphi_{n_1} \rangle \langle \varphi_{n_1'} \rangle. \tag{39}$$

The asymptotic decay $G^{(0)}_{n_1} \approx c e^{-man_1}$ for large n_1 defines the lightest mass, the inverse Compton wavelength in units of the UV cutoff, $ma = a/\xi$.

The numerical calculation are restricted to a finite volume where there are no phase transitions. Thus the lattice should be large enough to avoid the symmetry restoration by the flip-flops of the slow mode, the sudden changes of sign of the order parameter

$$\Phi = \frac{1}{N_L^3} \sum_n \phi_n \tag{40}$$

during the simulation. The lattice size $N_L = 100$ was used in the numerical work and no flip-flop was seen.

A. Hysteresis cycles

In order to check the convergence of the Monte-Carlo iterations two hysteresis cycles were made in g_{L4} with the results shown in Fig. 8. The simulation started with an ordered configuration $\phi_n = 0$ and g_{L4} was moved through the values $g_{L4} = -0.01n$, $n = 0, \ldots, 14$ by executing 1000 sweeps with fixed $g_{L2} = 0.01$, $g_{L6} = 0.1$ in such a manner that the last configuration at a g_{L4} value was used as the initial configuration for the next g_{L4} point. At the end the final configuration was taken and the values $g_{L4} = -0.115 + 0.01n$ were visited in an opposite move in a similar sequential manner. Another hysteresis cycle was performed with at most 250000 sweeps at the same g_{L4} values but in this case the initial configuration was $\phi_n = 0$ and 5 at $g_{L4} = -0.01n$ and $g_{L4} = -0.115 + 0.01n$, respectively. The iterations stopped when the order parameter converged in the last 40000 sweeps in the energetically preferred phase. This rearrangement allows to see the speed of convergence of the simulation.

The action S and the order parameter Φ, depicted in Figs. 8(a) and 8(b), represent an UV and an IR observable

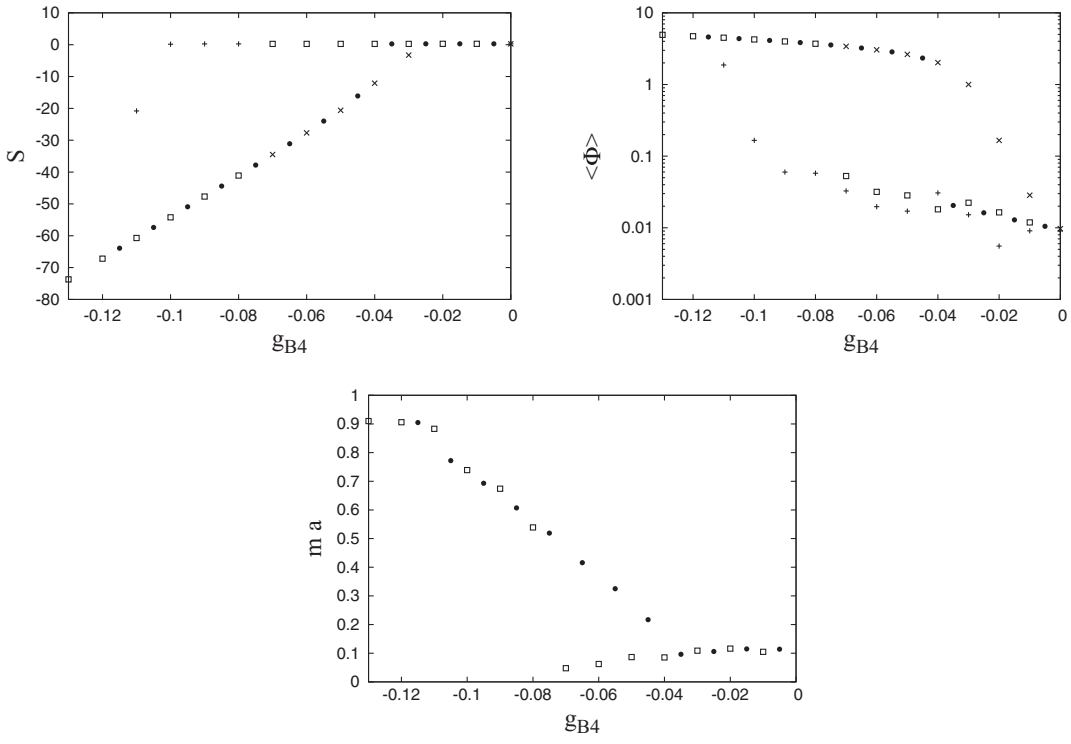

FIG. 8. The hysteresis cycle for the action S, the order parameter Φ, and the inverse mass $1/ma$ in the coupling constant g_{L4} with $g_{L2} = 0.01$ and $g_{L6} = 0.1$. The symbols plus (square) and times (black dot) indicate the down and the up moving part of the cycle with 1000 (at most 250000) sweeps at each point. The inverse mass is shown only for the longer iteration series.

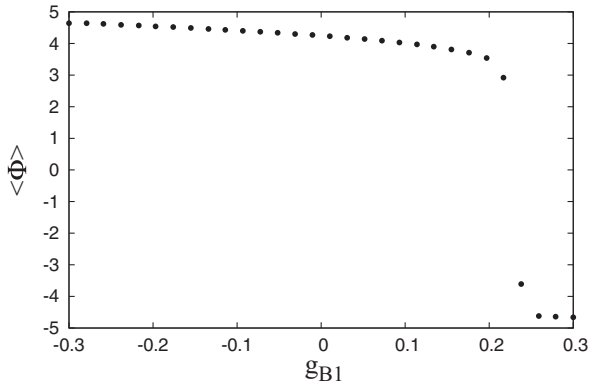

FIG. 9. Half of the hysteresis cycle of the order parameter in g_{L1} with the bare parameters are $g_{L2} = 0.01$, $g_{L4} = 0$, and $g_{L6} = 0.1$.

with a much faster convergence for the former than for the latter. The approximately linear dependence of the action on g_{L4} can be understood by assuming that the fluctuations are weak at the scale of the lattice spacing since the expectation value of the order parameter is approximately g_{L4} independent within this range according to Fig. 8(b).

The first order phase transition behind the hysteresis cycle Fig. 8 separates the disordered ($\langle\Phi\rangle = 0$) and the ordered ($\langle\Phi\rangle \neq 0$) phases. Another first order transition in this theory is between the two ordered vacua, $\langle\Phi\rangle = \pm\Phi_0$, its signature is the hysteresis cycle plotted in Fig. 9. Here g_{L1} was moved through the interval $-0.3 < g_{L1} < 0.3$ from left to right in the symmetry broken phase in a sequential manner as in the case of the previous hysteresis cycle with 1000 iterations. In the other half of the cycle, not shown in the figure, one finds the same curve with the transformation $g_{L1} \to -g_{L1}$.

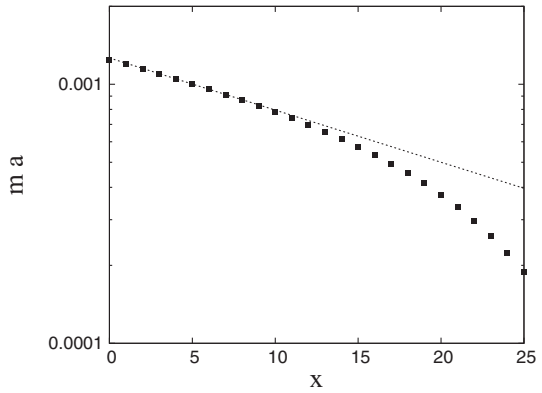

FIG. 10. The connected φ_{n1} correlation function denoted by squares and its fit indicated by dotted line for $g_{L2} = 0.01$, $g_{L4} = -0.07$, and $g_{L6} = 0.1$. The best estimate of the error bar is the difference between the average at $n_1 = 25$ and the exponential fit. The figure is based on the dataset corresponding to the last 200 points of the series shown in Fig. 11.

B. Limitation in the UV

The rich phase structure predicted by the renormalization group method is due to the strong renormalization. To recover the fine balance between the diferent contributions to the beta functions one has to suppress the lattice artefacts of the free lattice propagator, achieved by performing the continuum limit $\xi = 1/ma \to \infty$ diverges. The calculation of the mass gap is shown for $g_{L4} = -0.07$ in Fig. 10, the result of a fit of the logarithm of the connected correlation function (39) by a linear function of the distance. The mass gap, obtained by such fitting, is shown for the full hysteresis cycle on Fig. 8(c). The statistical errors are smaller than the symbol size and the systematic errors can be estimated by the difference between the two hysteresis series.

The lesson is that we are far from the continuum limit when the order parameter is nonvanishing. One could reduce the mass by going closer to the Gaussian fixed point but a large amplitude, slow wandering of the order parameter creates a serious numerical problems. Such a critical slowing down close to a second order phase transition can in principle be reduced by Fourier acceleration of the slow modes [47], multigrid [48], and cluster update [49].

C. Limitation in the IR

A fully converged simulation produces no hysteresis cycle which arises from the simulation getting stuck in the false vacuum. Thus Figs. 8 and 9 report a serious slow down of the convergence around first order phase transitions, a well known limitation of the Monte-Carlo method.

The point $\phi = 0$ remains a local minimum of the bare potential for any g_{L4}. However the finite length Monte-Carlo iteration series lead to the stable vacuum with nonvanishing order parameter only for sufficiently negative g_{L4}, beyond the true transition point. A few typical Monte-Carlo series are shown in Fig. 11, they represent three points on Fig. 8(b). The simulation time needed to find the energetically stable true vacuum is supposed to increase exponentially with the volume within the interval $-0.09 < g_{L4} < -0.07$. Once the stable vacuum is reached the system stays there. There is a similar problem to find the transition by starting from the ordered phase with nonvanishing order parameter. It is interesting that this part of the cycle with more iterations closes at the tree-level transition point at $g_{L4} = g_{4\mathrm{tr}} = -0.04$. This might be an accident since the renormalization between the lattice spacing and the size of the lattice is very strong, see Sec. V D below. The lesson of Fig. 9 is similar since the simulation with finite iteration series find the transition only when the true vacuum is much below the false one.

The hysteresis cycle of Fig. 4 covers the region where one expects the second first order transition predicted by the renormalization group method. as far as the second order phase transitions of Fig. 6 are concerned, one needs

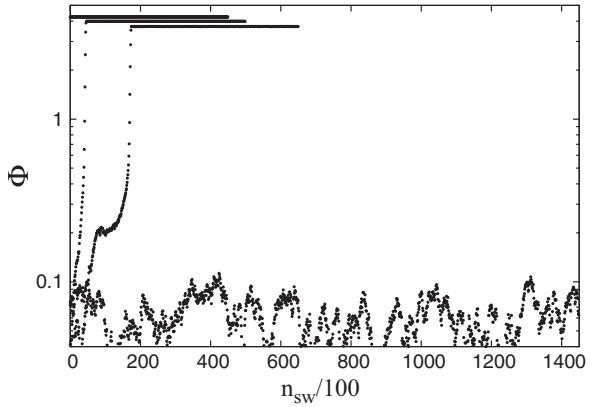

FIG. 11. The Monte-Carlo sequences of the order parameter. A point corresponds to the absolute magnitude of the order parameter averaged over 100 sweeps. The bare parameters are $g_{L2} = 0.01$, $g_{L6} = 0.1$, and $g_{L4} = -0.07, -0.08, -0.09$, and -0.1. The order parameter increases as g_{L4} moves toward the negative direction.

small bare parameters. However the order parameter follows a slow but large amplitude oscillation during the simulation in the symmetric phase because the restoring force at $\Phi = 0$, $U'(0)$, is very weak and one encounters a slow down similar to the one arising in the continuum limit.

D. Droplets

The droplets are supposed to provide the driving force of a first order transition [7–10] hence their presence is crucial in the Monte-Carlo simulation. Their identification during the iteration serves two goals in the same time. First, it may help to find the phase coexisting region, a problem raised in Sec. IV D, and it might help to design improved update schemes with faster convergence.

It is easy to see whether the droplets are present in the simulation by calculating the histogram of the local field variable. For this end a hysteresis cycle was made by moving g_{B4} through the values $-0.01n$, $n = 3, 4, \ldots, 8$ and performing twice 40000 sweeps with initial configurations $\phi_n = 0$ and $\phi_n = 5$ at each point. This hysteresis cycle closes at the end points, at $g_{L4} = -0.03$ and -0.08 but the Monte-Carlo series are not convergent in between, cf. Fig. 8. The histogram, the probability distribution of ϕ_n, is calculated for $\phi \in [-\Phi_0, \Phi_0]$ by dividing the interval $[-\Phi_0, \Phi_0]$ into N_h subinterval and by counting the number of field variable found within each subinterval.

The normalized histograms with $\Phi = 8$ and $N_h = 200$ are shown in Fig. 12(a) at the six values of g_{L4}. The histograms corresponding to the initial configuration $\phi_n = 0$ peak around zero and are undistinguishable on the plot with linear scale for Φ except the one at $g_{L4} = -0.08$ which displays two peaks, indicating that the system found the way to the energetically stable vacuum approximatively at half-time of the iteration series. The histograms of the initial configuration $\phi_n = 5$ show the gradual decrease of the average Φ as g_{L4} moves in the positive direction, the last histogram at $g_{L4} = -0.03$ is already in the disordered phase and is undistinguishable from the other curves peaking around zero.

The double peak of the histogram at $g_L = -0.8$ with the initial condition $\phi_n = 0$ shows that both ordered and disordered vacuum droplets occur in this Monte-Carlo series. To find out whether they show up in the same configuration we zoom into that part of the Monte-Carlo iteration where Φ changes fast, the result being displayed in Fig. 12(b). The part of the series where the distribution displays double peak with gradually changing maximal values proves the Φ converges by inhomogeneous droplets formation rather than by a continuous homogeneous drift of a single peak probability distribution. This suggest a qualitative similarity between the coexisting region and such subseries of the simulation where the order parameter jumps between the phases. One thus arrives at the result that the droplets are absent or play a negligible role in the long, converged Monte-Carlo series. An immediate result is the

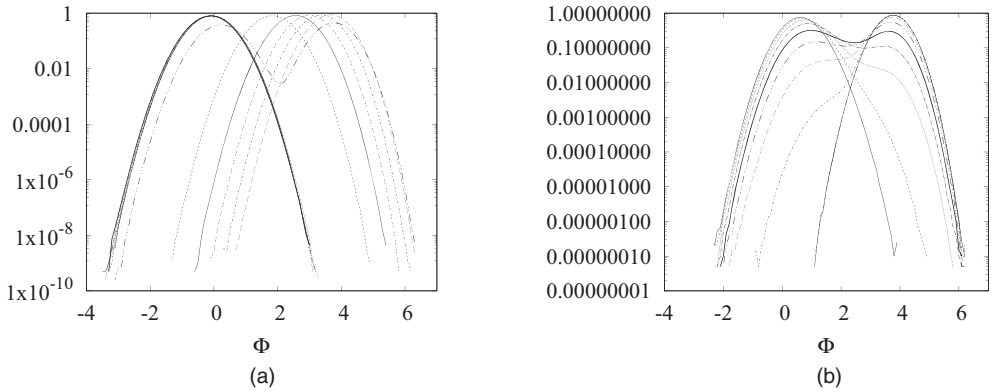

FIG. 12. (a) The normalized distributions of ϕ_n. The bare parameters are $g_{L2} = 0.01$, $g_{B4} = -0.01n$, $n = 3, 4, \ldots, 9$, $g_{L6} = 0.1$. (b) The evolution of the histogram at $g_{L4} = -0.8$ with initial configuration $\phi_n = 0$ by collecting statistics for the sweeps $190000 + 1000n \leq n_{sw} < 191000 + 1000n$ where $n = 0, \ldots, 9$. No local field was found at values without historgram curve.

conjecture that the phase coexisting region collapses to a point in the parameter space g_{Ln}.

E. Improving the Monte-Carlo algorithms

No droplet was found in the relaxed Monte-Carlo series hence one expects that their inclusion should speed up the algorithm around the phase transition. But such an improvement opens a new question about ergodicity: The dynamical description of phase transitions is based on the separation of the short and the long characteristic timescales. The short microscopic timescales converge and the long timescales of certain collective modes diverge and generate discontinuities between the UV and the IR parameters in the thermodynamical limit. The phase transition is understood dynamically as an approximation where such slow modes are kept time independent. The view leads to the static characterization of a phase transition as a particular breakdown of ergodicity and the statistical ensembles should be appropriately redefined. The troublesome point is that the slow dynamical modes are usually slow in the simulation time, too. Hence the speed up the slow modes in the simulation time may change the handling of the slow dynamical modes and lead to an inappropriate breakdown of ergodicity.

Another way to phrase the problem is to recall the difference between the bare and the renormalized parameters of the theory. On the one hand, the Monte-Carlo algorithm is defined on the level of the bare action characterizing the dynamics close to the UV cutoff. On the other hand, the slow modes to speed up are nonlocal and their dynamics is expressed in terms of renormalized IR parameters. Thus the proper improvement of the algorithm must include the relation between the UV and the IR parameters.

There are several tested proposals to reduce the critical slow down in the vicinity of second order phase transitions. The replacement of the Monte-Carlo iteration series by an artificial, supposedly ergodic, dynamics allows us to use different discrete time steps for different modes of the theory [47,50]. The choice of larger time step for the long wavelength Fourier modes of the space-time lattice can strongly reduce the relaxation time in the vicinity of a critical point. One can introduce the update of Kadanoff's block variables and interpret the resulting random walk as a multigrid generalization of the Monte-Carlo algorithm [48]. The direct introduction of the nonlocal update of a cluster of parallel spins [49] became a generally used acceleration method close to the critical point of lattice spin models. As long as the modification of a local Monte-Carlo update is restricted to scales close to the lattice spacing, as in the multigrid Monte-Carlo and the cluster update schemes, the breakdown of ergodicity remains unchanged at a second order phase transition. However the Fourier acceleration method applied for the long range collective modes opens the question whether the artificial IR dynamics breaks ergodicity just in the desired manner.

While the multigrid and the cluster algorithms improve the convergence around critical points we believe that similar nonlocal updates run into a problem at a first order transition. The reason can be demonstrated by a very simple cluster update step to be offered when the bare potential supports several local minima $g_{L4} < -\sqrt{6 g_{L2} g_{L6}/5}$: Within a box of size N_b we reflect the local field variable across $\pm\phi_m/2$, $\phi_n \to \mathrm{sign}(\phi_n)\phi_m - \phi_n$. The size N_b is chosen to bring the phenomenological droplet action,

$$S_d = N_b^3[U(\min(\phi_m,0)) - U(\max(\phi_m,0))] + 3N_b^2\bar{\phi}^2, \quad (41)$$

as close to zero as possible from below to reach reasonable acceptance ratio. Such a procedure gives $N_b = [3\phi_0^2/\Delta U] + 1$ where $[x]$ stands for the integer part of x and $\bar{\phi}$ is a fixed parameter. This tentative update is mentioned here only for the sake of the argument, the realistic version needs further refinement to reach better acceptance ratio. The point is that the domain where the local field variables are changed should approach the total lattice volume close to the unrenormalized tree-level phase boundary. Hence we enter into the modification of the update at arbitrary long length scales without any information about the renormalized long range dynamics which determines the true transition point.

VI. SUMMARY

The renormalization group method was used to sketch the phase structure of the three dimensional ϕ^6 scalar field theory. The order parameter is obtained by integrating the Wegner-Houghton equation for the bare potential as the UV cutoff is lowered. The usual method, based on the beta functions at vanishing order parameter, produces an unbounded potential from below at a finite value of the cutoff and prevents us from reaching the IR regime. An improved implementation of the Wegner-Houghton equation is used which is based on a weighted average of the beta functions at the different minima of the potential and provides a stable renormalized trajectory. The absolute minimum plays an increasing role in the weighted average as the cutoff is lowered and the location of the absolute minimum of the potential at the IR end point can be identified with the expectation value of the order parameter.

One finds the Wilson-Fisher fixed point at a different location and several phase transitions by the help of this procedure. The absolute minimum of the potential stays at zero or remains at a nonzero value along the renormalized trajectories deeply in the symmetric and symmetry broken side of the first order transition, respectively. But close to the first order transition line a new radiative corrections generated first phase transitions arises. A remarkable feature of the strip between the two transitions is that

the potential is locked into a degenerate minimum shape within a finite scale window of the running cutoff. The degenerate minima of the potential make this region reminiscent of usual the phase coexisting region.

The mass of elementary excitations is determined in the symmetry broken phase mainly by the order parameter and such a dynamically generated mass was found to be larger than the UV cutoff. By assuming that this result survives the Wick rotation back to real time where the UV-IR crossover marks the separation of the relativistic and nonrelativistic domain one is left with the conjecture that the first order symmetry breaking is an intrinsically nonrelativistic phenomenon in this model.

The symmetric phase has a surprising feature, as well, it supports a new second order transition at the spontaneous breakdown of the symmetry $\phi \to -\phi$ due to the local minima of the potential appearing for sufficiently negative quartic coupling constant. Several other phase transitions are expected due to the competition of different terms in the potential.

The phase structure is checked by Monte-Carlo simulation but the result is inconclusive owing to the presence of lattice artefacts modifying the scaling behavior, and the slowness of the convergence of the random walk just in the region of the parameter space where the new phase transitions may appear. It is pointed out that the known methods to speed up a local update algorithm by nonlocal steps have to be refined close to a first order phase transition.

We are therefore left with the conjecture of a more involved phase diagram of the ϕ^6 model and a number of problems waiting for clarification, we mention but few of them: How does the phase structure change by extending the calculation for higher order polynomials? What kind of further phase transitions occur as the result of the competition of different nonquadratic terms in the potential? How to reach the phase mixing region of the model? Is there first order phase transition with mass below the cutoff? How to improve the Monte-Carlo algorithm to go closer to the first order transition?

[1] E. Stückelberg and A. Peterman, Helv. Phys. Acta **24**, 317 (1951), https://inspirehep.net/literature/42640.
[2] N. N. Bogoliubov and D. V. Shirkov, *Introduction to the Theory of Quantized Fields* (Wiley-Interscience, New York, 1959).
[3] J. W. Essam and M. E. Fischer, J. Chem. Phys. **38**, 802 (1963).
[4] B. Widom, J. Chem. Phys. **43**, 3892 (1965).
[5] L. Kadanoff, Phys. Phys. Fiz. **2**, 263 (1966).
[6] K. G. Wilson and J. Kogut, Phys. Rep. **12**, 75 (1974).
[7] J. S. Langer, Ann. Phys. (N.Y.) **41**, 108 (1967).
[8] M. E. Fischer, Phys. Phys. Fiz. **3**, 255 (1967).
[9] M. B. Voloshin, I. Y. Kobzarev, and L. B. Okun, Sov. J. Nucl. Phys. **20**, 644 (1975), https://inspirehep.net/literature/88934.
[10] K. Binder, Rep. Prog. Phys. **50**, 783 (1987).
[11] K. G. Wilson and M. E. Fisher, Phys. Rev. Lett. **28**, 240 (1972).
[12] J. M. Kosterlitz and D. J. Thouless, J. Phys. C **6**, 1181 (1973).
[13] J. Alexandre, V. Branchina, and J. Polonyi, Phys. Rev. D **58**, 016002 (1998).
[14] F. J. Wegner and A. Houghton, Phys. Rev. A **8**, 401 (1973).
[15] J. Polchinski, Nucl. Phys. **B231**, 269 (1984).
[16] C. Wetterich, Phys. Lett. B **301**, 90 (1993).
[17] B. I. Halpern, T. C. Lubensky, and S-K. Ma, Phys. Rev. Lett. **32**, 292 (1974).
[18] S. Coleman and E. Weinberg, Phys. Rev. D **7**, 1888 (1973).
[19] D. J. Wallace, J. Phys. C **6**, 1390 (1973).
[20] J. Rudnick, Phys. Rev. B **18**, 1406 (1978).
[21] B. Nienhuios and M. Nauenberg, Phys. Rev. Lett. **35**, 477 (1975).
[22] F. Zhong and Q. Chen, Phys. Rev. Lett. **95**, 175701 (2005).
[23] W. Klein, D. J. Wallace, and R. K. Zia, Phys. Rev. Lett. **37**, 639 (1976).
[24] V. Privman and M. E. Fischer, J. Stat. Phys. **33**, 385 (1983).
[25] A. Hasenfratz and P. Hasenfratz, Nucl. Phys. **B295**, 1 (1988).
[26] N. Liang and F. Zhong, Front. Phys. **12**, 126403 (2017).
[27] A Parola, D. Pini, and L. Reatto, Phys. Rev. E **48**, 3321 (1993).
[28] K. I. Aoki, S. I. Kumamoto, and M. Yamada, Nucl. Phys. **B931**, 105 (2018).
[29] S. Bornholt, N. Tetradis, and C. Wetterich, Phys. Lett. B **348**, 89 (1994).
[30] S. Bornholt, N. Tetradis, and C. Wetterich, Phys. Rev. D **53**, 4552 (1996).
[31] J. Berges, N. Tetradis, and C. Wetterich, Phys. Lett. B **393**, 387 (1997).
[32] J. Berges and C. Wetterich, Nucl. Phys. **B487**, 675 (1997).
[33] N. Tetradis, Phys. Lett. B **431**, 380 (1998).
[34] A. Strumia and N. Tetradis, Nucl. Phys. **B542**, 719 (1999).
[35] A. Strumia and N. Tetradis, Nucl. Phys. **B554**, 697 (1999).
[36] P. Jakubczyk, Phys. Rev. B **79**, 125115 (2009).
[37] M. Reichert, A. Eichhorn, H. Gies, J. M. Pawlowski, T. Plehn, and M. M. Scherer, Phys. Rev. D **97**, 075008 (2018).
[38] R. Gersch, J. Reiss, and C. Honerkamp, New J. Phys. **8**, 320 (2006).
[39] J. Alexandre, V. Branchina, and J. Polonyi, Phys. Lett. B **445**, 351 (1999).
[40] V. Pangon, S. Nagy, J. Polonyi, and K. Sailer, Int. J. Mod. Phys. A **26**, 1327 (2011).
[41] E. Grossi and N. Wink, SciPost Phys. Core **6**, 071 (2023).

[42] A. Koenigstein, M. J. Steil, N. Wink, E. Grossi, J. Braun, M. Buballa, and D. H. Rischke, Phys. Rev. D **106**, 065012 (2022).
[43] F. Ihssen, J. Pawlowski, F. Sattler, and N. Wink, Comput. Phys. Commun. **300**, 109182 (2024).
[44] T. Morris, Phys. Lett. B **334**, 355 (1994).
[45] K. Halpern and K. Huang, Phys. Rev. D **53**, 3252 (1996).
[46] T. Morris, Phys. Rev. Lett. **77**, 1658 (1996).
[47] G. G. Batrouni, G. R. Katz, A. S. Kronfeld, G. P. Lepage, B. Svetitsky, and K. G. Wilson, Phys. Rev. D **32**, 2736 (1985).
[48] J. Goodman and A. D. Sokal, Phys. Rev. Lett. **56**, 1015 (1986).
[49] R. H. Swendsen and J. S. Wang, Phys. Rev. Lett. **58**, 86 (1987).
[50] S. Duane, Nucl. Phys. **B257**, 652 (1985).